Detection and Quantification of Large-Vessel Inflammation with ^{11}C-(*R*)-PK11195 PET/CT

Frederic Lamare[1], Rainer Hinz[2], Oliver Gaemperli[1], Francesca Pugliese[1], Justin C. Mason[3], Terence Spinks[4], Paolo G. Camici[1,5], and Ornella E. Rimoldi[1,6]

[1]MRC Clinical Sciences Centre and National Heart and Lung Institute, Imperial College, Hammersmith Campus, London, United Kingdom; [2]Wolfson Molecular Imaging Centre, Manchester, United Kingdom; [3]Cardiovascular Sciences, Bywaters Center for Vascular Inflammation, National Heart and Lung Institute, Imperial College, Hammersmith Campus, London, United Kingdom; [4]GE Imanet, Hammersmith Hospital, London, United Kingdom; [5]Università Vita e Salute San Raffaele Milano, Italy; and [6]IFC CNR Pisa, Pisa, Italy

We investigated whether PET/CT angiography using ^{11}C-(*R*)-PK11195, a selective ligand for the translocator protein (18 kDa) expressed in activated macrophages, could allow imaging and quantification of arterial wall inflammation in patients with large-vessel vasculitis. **Methods:** Seven patients with systemic inflammatory disorders (3 symptomatic patients with clinical suspicion of active vasculitis and 4 asymptomatic patients) underwent PET with ^{11}C-(*R*)-PK11195 and CT angiography to colocalize arterial wall uptake of ^{11}C-(*R*)-PK11195. Tissue regions of interest were defined in bone marrow, lung parenchyma, wall of the ascending aorta, aortic arch, and descending aorta. Blood-derived and image-derived input functions (IFs) were generated. A reversible 1-tissue compartment with 2 kinetic rate constants and a fractional blood volume term were used to fit the time–activity curves to calculate total volume of distribution (V_T). The correlation between V_T and standardized uptake values was assessed. **Results:** V_T was significantly higher in symptomatic than in asymptomatic patients using both image-derived total plasma IF (0.55 ± 0.15 vs. 0.27 ± 0.12, $P = 0.009$) and image-derived parent plasma IF (1.40 ± 0.50 vs. 0.58 ± 0.25, $P = 0.018$). A good correlation was observed between V_T and standardized uptake value ($R = 0.79$; $P = 0.03$). **Conclusion:** ^{11}C-(*R*)-PK11195 imaging allows visualization of macrophage infiltration in inflamed arterial walls. Tracer uptake can be quantified with image-derived IF without the need for metabolite corrections and evaluated semiquantitatively with standardized uptake values.

Key Words: large-vessel vasculitides; atherosclerosis; ^{11}C-(*R*)-PK11195; positron emission tomography; CT angiography

J Nucl Med 2011; 52:33–39
DOI: 10.2967/jnumed.110.079038

Molecular imaging with PET and ^{18}F-FDG has proven suitable to detect vascular inflammation mainly in vascular beds that are not accessible for biopsy (*1,2*). The increasing use of hybrid PET scanners and concomitant CT angiography offers the advantage of a precise colocalization of the signal onto a clearly delineated vessel wall anatomy (*3–5*).

[*N*-methyl-^{11}C]-(*R*)-1-(2-chlorophenyl)-*N*-(1-methylpropyl)-3-isoquinoline carboxamide, or ^{11}C-(*R*)-PK11195, is a radioligand that specifically binds to the translocator protein (18 kDa), formerly also referred to as ω_3 receptor, or peripheral benzodiazepine receptor (*6*). High levels of translocator protein (18 kDa) are expressed in macrophages when activated by cytokines, making them a potential imaging target for large-vessel inflammation (*5,7,8*).

Over the last 2 decades, ^{11}C-(*R*)-PK11195 has been extensively used to study neuroinflammation in a wide range of brain disorders (*9–14*). The quantitative analysis of ^{11}C-(*R*)-PK11195 brain studies has been challenging because of the relatively small amount of specific binding, the absence of an anatomically defined reference region in the brain, and the specific binding of ^{11}C-(*R*)-PK11195 in brain blood vessels (*15–19*). Therefore, specific methodology for the analysis of dynamic brain PET studies with ^{11}C-(*R*)-PK11195 has been developed to extract reference tissue kinetics with cluster analysis (*9,17*) and to account for vascular activity in the reference region (*18*).

Quantitative studies of inflammatory processes in the lungs (*20,21*) and joints (*22,23*) have been performed by means of kinetic modeling with plasma input functions (IFs) derived from direct blood sampling (*20–22*) or obtained from the blood pool in the image (*24*). The tissue uptake was expressed as tissue-over-plasma activity concentration ratio, and only the most recent of these studies used compartmental modeling to obtain total volume of distribution (V_T) estimates (*22*).

The discriminatory power of this tracer was assessed comparing patients with active giant cell arteritis and Takayasu's arteritis of the great vessels with patients with systemic lupus erythematosus.

The primary objective was to develop a quantitative methodology for imaging large-vessel inflammation with ^{11}C-(*R*)-PK11195 deriving both plasma and image IFs, alongside the

Received May 11, 2010; revision accepted Oct. 18, 2010.
For correspondence or reprints contact: Ornella E. Rimoldi, MRC Clinical Sciences Centre, Hammersmith Hospital, DuCane Rd., London W12 0NN, U.K.
E-mail: rimoldi.ornella@hsr.it

question of whether the plasma IF needs correction for the fraction of unmetabolized radioligand.

Dynamic scanning with continuous blood sampling might not be feasible in a solely clinical environment. Hence, to explore the agreement of quantitative and semiquantitative measurements, we compared the performance of the standardized uptake value (SUV) (*5*) with the results of quantitative kinetic analysis.

MATERIALS AND METHODS

Study Population

From Hammersmith Hospital rheumatology outpatient clinic, 7 patients with the systemic inflammatory disorders giant cell arteritis, Takayasu's arteritis, or systemic lupus erythematosus were enrolled. Three patients had signs and symptoms of active vasculitis, defined as onset within the previous 6 wk of any of the following symptoms: visual disturbance, headache, bruit or vascular pain/tenderness, new claudication, fever, night sweats, or arthralgia. The remaining 4 patients were asymptomatic. Exclusion criteria for all patients were known intolerance to iodinated contrast agent, inability to lie flat, a prior PET scan within 1 y of the study, age lower than 25 y or higher than 75 y, or claustrophobia. The study protocol was approved by the local Research Ethics Committee, and all patients gave written informed consent. Radiation exposure was licensed by the U.K. Administration of Radioactive Substances Advisory Committee.

PET/CT Protocol

Imaging was performed using a 16-slice PET/CT scanner (Discovery RX; GE Healthcare) with a 15-cm field of view positioned in the region of the aortic arch and its branches. A low-dose CT scan was acquired in helical mode for attenuation correction with the following parameters: 120 kV, 20 mAs, 8 × 2.5-mm slice thickness, pitch of 1.675, and 0.5-s rotation time. After intravenous injection of 6.85 MBq of ^{11}C-(*R*)-PK11195 per kilogram of body weight, PET emission data were acquired over 60 min in list-mode format and rebinned into 18 temporal frames (30-s background, 1 × 15 s, 1 × 5 s, 1 × 10 s, 1 × 30 s, 4 × 60 s, 7 × 300 s, and 2 × 600 s).

After the PET scan, CT angiography was performed with the same field of view as the PET scan. A bolus of 70 mL of contrast material (Ultravist 370; Schering) was injected at a rate of 3.5 mL/s into an antecubital vein. The CT angiography acquisition parameters were 120 kV, 180 mAs, 16 × 0.625-mm slice thickness, pitch of 1.0, and 0.5-s rotation time.

Image Reconstructions

All PET emission scans were normalized for detector inhomogeneity and corrected for randoms, dead time, scatter, and attenuation. Two different image reconstructions were performed. First, the 18 frames of the dynamic emission scans were reconstructed using the 3-dimensional reprojection algorithm (*25*) with the ramp filter set to Nyquist frequency to obtain fully quantitative images. Second, the dynamic frames were also reconstructed using an ordered-subset expectation maximization algorithm with 2 iterations and 21 subsets (*26*) to obtain images with superior visual quality allowing manual definition of regions of interest (ROIs). For both reconstruction algorithms, a matrix size of 128 × 128 × 47 voxels was used, with a voxel size of 2.28 × 2.28 × 3.27 mm.

Initial reconstruction parameters for CT angiography were 0.625-mm slice thickness, 0.625-mm increment, 30-cm-wide reconstruction field of view, window width of 300 Hounsfield units, and window level of 30 Hounsfield units.

Definition of ROIs

ROIs were defined on the PET images overlaid with the rebinned CT images using dedicated software developed in-house within Matlab 6.5 (The MathWorks) (Data Supplement I provides full details; supplemental materials are available online only at http://jnm.snmjournals.org).

Blood Sampling and Generation of the Plasma IF

Arterialized venous blood was sampled continuously for the initial 20 min of the scan from the antecubital vein of a heated arm or the dorsal vein of a heated hand.

Arterialization was confirmed by a venous blood oxygen partial pressure greater than 60 mm Hg (*27*). Plasma samples were analyzed for radiolabeled metabolites (Data Supplement I provides full details of the sampling protocol).

^{11}C-(*R*)-PK11195 has never been evaluated for large-vessel disease, and it is unknown whether radiolabeled metabolites reach the target region. Therefore, 2 different IFs were generated: they represent either the total activity concentration in plasma (total plasma) or the activity concentration in plasma due to parent ^{11}C-(*R*)-PK11195 (parent plasma). For the generation of the plasma IFs, the time course of the plasma-over-blood (POB) ratio obtained from the 8 discrete arterialized venous samples was fitted to a straight-line model:

$$\mathrm{POB}(t) = p_0 + p_1 \cdot t \qquad \text{Eq. 1}$$

where p_0 and p_1 are the coefficients of the linear model and t is time. The measurement of the arterialized venous whole-blood activity obtained from the continuous detector system was subsequently multiplied by that ratio to obtain a total plasma activity curve for the first 20 min of the scan. This curve was then combined with the discrete plasma activity concentration measurements at 20, 30, 40, 50, and 60 min to form an IF describing the total plasma activity concentration for the entire scan. The mathematic model for the description of the amount of parent compound in plasma was the following equation:

$$\mathrm{Parent}\,(t) = (1 - q_2) \cdot \exp\,(-\,q_1 \cdot t) + q_2 - q_3 \cdot t \qquad \text{Eq. 2}$$

with q_1, q_2, and q_3 being greater than 0. This function describes an exponential approach to a falling straight line, beginning at 1 for time $t = 0$. The IF of the activity concentration due to the parent ^{11}C-(*R*)-PK11195 in plasma was created by multiplying the total plasma activity IF by the parent fraction model function:

$$\mathrm{IF}_{\text{parent plasma}}(t) = \mathrm{IF}_{\text{total plasma}}(t) \times \text{parent}\ \ (t) \qquad \text{Eq. 3}$$

The models for the POB ratio and for the parent fraction were used for both the blood sampler–derived IFs (BSIFs) and the image-derived IFs (IDIFs). This latter was cross-calibrated with the first 4 discrete blood samples, corresponding to the first 20 min of the scan. The IFs were generated using dedicated software developed in-house within Matlab 6.5.

Kinetic Analysis

To fit the computed time–activity curves, we have used a reversible 1-tissue compartment with 2 kinetic rate constants and a fractional blood volume term proposed by Kropholler et al. (*22*).

This model describes the uptake of radiotracer from plasma into tissue (K_1), and washout from tissue (k_2). Parameters of interest evaluated were the V_T defined as $\frac{K_1}{k_2}$, as well as the blood volume. This latter parameter provided correction for spillover from the vasculature.

To discard noisy data, we included only the results with a coefficient of variation (mean\SD) below 50% . Only 2 of 116 fits were affected.

The delay between the arrival of the ^{11}C-(*R*)-PK11195 bolus at the organ of interest and the IF was estimated for each individual ROI. The tracer arrival delay was determined by varying the discrete delay parameter over a predefined set of values and performing the model fit. The delay value that corresponded to the smallest weighted residual sum of squared errors was chosen (*28*).

SUVs were calculated as the average tissue activity concentration in each ROI (in Bq/mL) divided by total injected activity per body weight (in Bq/g).

Data are reported as mean values ± SD, and comparisons were made by means of the unpaired 2-tailed Student *t* test. Correlation between SUV and V_T was tested by means of Pearson correlation. Statistical analyses were performed using the Statistical Package for Social Science, version 16.0.1 (SPSS Inc.). A *P* value of less than 0.05 was considered statistically significant.

RESULTS

IFs

A representative comparison between the total-blood IDIF and the total-blood BSIF from 1 subject (Fig. 1) shows that the peak value of the BSIF is only about 30% of the peak value of the IDIF. However, because the IDIF is derived from framed images, its peak value may still be underestimated. The BSIF has a lower kurtosis and is skewed to the right.

The area under the curve formed by the IDIF and the BSIF (corrected for radioactive decay) was computed for the 7 patients (Supplemental Table 1 and Data Supplement I). The mean difference between the 2 areas under the curve over the whole study population was 30%, 13%, and 9.8% at 5, 30, and 60 min after the injection, respectively. This observation indicates that the BSIF is likely to be the dispersed representation of the arterial IF. These pronounced differences between arterial and venous blood were expected for a high-extraction tracer such as ^{11}C-(*R*)-PK11195 (*29*).

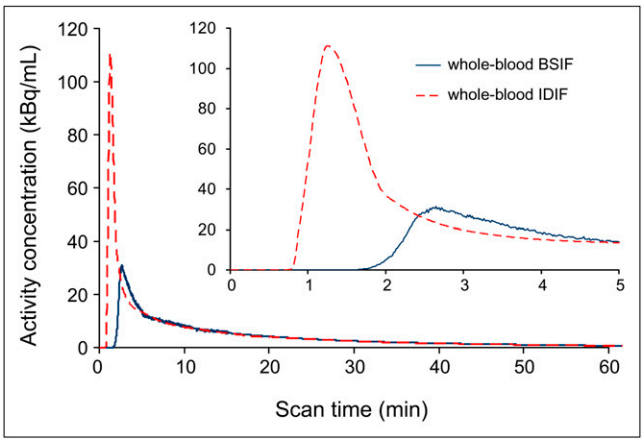

FIGURE 1. Representative example of whole-blood BSIF and IDIF derived from 1 asymptomatic patient. Dispersion of whole-blood BSIF, in comparison with IDIF, can clearly be seen.

The POB ratio changed little over the duration of the PET scan and did not show any significant difference among subjects (further details are presented in Data Supplement II and Fig. 2) The population mean parent fraction in plasma decreased from 68.0% ± 6.6% at 5 min to 29.1% ± 5.7% at 60 min after injection (Fig. 2). No significant difference was detected in the computed parent fractions in plasma at 5 and 60 min after injection between the 2 groups of patients ($P > 0.59$). The fits to the fraction of radioactivity originating from ^{11}C-(*R*)-PK11195 in plasma and metabolites were fitted using Equation 2.

Tracer Kinetic Modeling

Representative examples of ^{11}C-(*R*)-PK11195 uptake in an asymptomatic (A) and a symptomatic patient (B) at the level of the aortic arch are shown in Figure 3. The comparison of the time–activity curves of the aortic vessel wall shows that, after the peak, the activity concentration in a symptomatic patient (D) is 2-fold that in an asymptomatic patient (C).

For all 5 different tissue regions, the data were fitted using 4 different IFs: either total-plasma BSIF or IDIF or parent-plasma BSIF or IDIF. The tracer arrival delay values are reported in Data Supplement II and Supplemental Table 2 for each region and IF for the entire study population. For 1 region and 1 type of IF (i.e., either BSIF or IDIF) there was no difference in the observed tracer arrival delay between total-plasma and parent-plasma IFs. With BSIF, the largest delay was observed in the lung region. In the aortic wall, the tracer arrival delay is smaller than for the lungs but similar to or greater than that in the bone marrow. When IDIFs are used, the tracer arrival delay for the aortic walls is close to zero because of the proximity of the tissue ROI and the ROI of the IDIF sampling. In the bone marrow, the tracer arrival delay may be negative because the activity in the IDIF rises before the activity in the bone ROI.

Tables 1 and 2 detail all the kinetic parameters estimated for the 2 cohorts of patients. The use of the BSIFs (total plasma or parent plasma) led to negative K_1 estimates and fractional blood volumes larger than 1 for the 3 aortic ROIs or the ROI drawn in the lung parenchyma. Consequently, the V_T estimates are negative for these regions. Using the IDIFs to fit the data from the aortic wall ROIs resulted in plausible estimates for K_1, blood volume, and V_T. Furthermore, in the last column of Tables 1 and 2, there is a significant reduction in the residual sum of squared errors in the aortic wall ROIs indicating a better fit of the data with IDIF than with BSIF. The time–activity curves fitted with the 1-tissue-compartment model were similar using either total-plasma or parent-plasma IDIF (further details are provided in Data Supplement II and Supplemental Fig. 3). V_T estimated from parent plasma tended to be higher in all the tissues (Eq. 3). In the aortic wall (Fig. 4), V_T was signifi-

TABLE 1
Parameter Estimates of Reversible 1-Tissue-Compartment Model for Symptomatic Patients

Region	IF	K_1 ($mL_{plasma} \cdot min^{-1} \cdot mL_{extravascular\ tissue}^{-1}$)	k_2 (min^{-1})	Blood volume	V_T ($mL_{plasma} \cdot mL_{extravascular\ tissue}^{-1}$)	Residual sum of square errors
Bone marrow	Total-plasma BSIF	0.086 ± 0.027	0.037 ± 0.027	0.123 ± 0.080	2.517 ± 0.689	3.498 ± 2.388
	Parent-plasma BSIF	0.141 ± 0.012	0.027 ± 0.007	0.125 ± 0.045	5.505 ± 1.794	3.631 ± 3.268
	Total-plasma IDIF	0.085 ± 0.034	0.037 ± 0.026	0.085 ± 0.094	2.500 ± 0.658	8.172 ± 7.568
	Parent-plasma IDIF	0.126 ± 0.018	0.025 ± 0.004	0.058 ± 0.036	5.258 ± 1.509	7.060 ± 4.875
Lung parenchyma	Total-plasma BSIF	0.010 ± 0.005	0.272 ± 0.324	0.392 ± 0.119	0.118 ± 0.108	2.092 ± 0.858
	Parent-plasma BSIF	0.013 ± 0.007	0.136 ± 0.147	0.388 ± 0.116	0.260 ± 0.249	2.032 ± 0.814
	Total-plasma IDIF	0.062 ± 0.032	0.414 ± 0.210	0.211 ± 0.035	0.153 ± 0.029	2.276 ± 3.198
	Parent-plasma IDIF	0.048 ± 0.020	0.211 ± 0.106	0.230 ± 0.045	0.246 ± 0.070	2.789 ± 3.763
Mean of aortic walls (descending, arch, ascending)	Total-plasma BSIF	0.013 ± 0.007	0.021 ± 0.019	0.544 ± 0.080	0.381 ± 0.406	14.189 ± 5.004
	Parent-plasma BSIF	0.018 ± 0.009	0.007 ± 0.016	0.539 ± 0.081	1.535 ± 1.518	14.411 ± 5.015
	Total-plasma IDIF	0.025 ± 0.016	0.046 ± 0.024	0.414 ± 0.055	0.549 ± 0.146	2.452 ± 1.462
	Parent-plasma IDIF	0.031 ± 0.019	0.025 ± 0.015	0.409 ± 0.055	1.400 ± 0.500	2.477 ± 1.457

Data are mean ± SD (n = 3). For all regions considered, kinetic parameters were computed for 4 BSIFs and IDIFs.

FIGURE 2. Manual blood sample analysis: POB ratio obtained from the 7 subjects (mean values with their SD are given for each of the 10 discrete arterial blood samples) (A); fraction of unmetabolized parent compound in arterial plasma (filled dots represent mean values and SD from the 7 PET studies) (B). Data previously reported in literature (*32–35*) are presented for comparison.

cantly higher in symptomatic patients with both total-plasma IDIF (0.55 ± 0.15 vs. 0.27 ± 0.12, $P = 0.009$) and parent-plasma IDIF (1.40 ± 0.50 vs. 0.58 ± 0.25, $P = 0.018$) The box plot showed no overlap in discriminating the 2 groups of patients.

SUV fell short of significance ($P = 0.07$) in discriminating symptomatic (1.21 ± 0.29) from asymptomatic (0.87 ± 0.1) patients. Nonetheless, as shown in Figure 5, SUV strongly correlated with total-plasma V_T ($R = 0.79$; $P = 0.036$) but not with parent-plasma V_T ($R = 0.53$; $P = 0.22$).

Symptomatic and asymptomatic patients did not differ in lung parenchyma either with total-plasma IDIF (0.15 ± 0.03 vs. 0.19 ± 0.04, respectively, P = not statistically significant [NS]) or with parent-plasma IDIF (0.25 ± 0.07 vs. 0.31 ± 0.12, respectively, P = NS). A similar pattern was seen in the bone marrow with total-plasma IDIF (2.50 ± 0.85 vs. 2.51 ± 0.54, respectively, P = NS) and with parent-plasma IDIF (5.26 ± 1.51 vs. 6.02 ± 0.93, respectively, P = NS).

DISCUSSION

Our findings demonstrate that active vasculitides in patients with systemic inflammatory disorders can be visualized (*5*) and quantified by macrophage targeting using ^{11}C-(*R*)-PK11195. The lack of significant uptake in asymptomatic patients confirms the sensitivity and selectivity of ^{11}C-(*R*)-PK11195 in imaging macrophage infiltrates (*30,31*).

As a probe suitable for brain imaging, ^{11}C-(*R*)-PK11195 is a highly lipophilic compound thought to cross the blood–brain barrier by passive diffusion. Because of the similar properties of the cell membranes of red blood cells, ^{11}C-(*R*)-PK11195 would also be expected to enter the red blood cells. However, a POB ratio of 1.38 at 5 min indicates that a

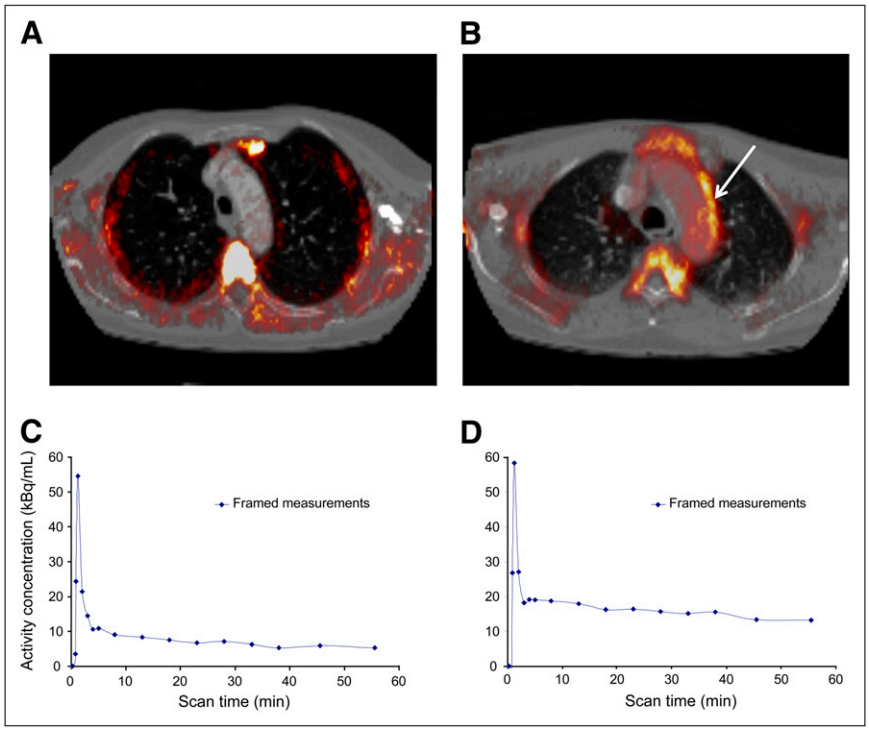

FIGURE 3. Example of asymptomatic (A) and symptomatic (B) patient. Gray-scale image is CT angiography coregistered with PET ordered-subset expectation maximization image. Each patient is shown in transverse view. Arrow indicates inflamed region of aortic arch. (C and D) Respective time–activity curves (corrected for radioactive decay) derived from aortic vessel wall.

large proportion of ^{11}C-(*R*)-PK11195 activity is concentrated in the plasma rather than in the red cells. The subsequent appearance of radiolabeled metabolites has only a small effect on the POB ratio, suggesting a similar partitioning of ^{11}C-(*R*)-PK11195 radioactivity and its radiolabeled metabolites between plasma and red blood cells. The POB ratio obtained in venous arterialized blood is approximately 10% smaller than the mean POB ratio of 1.55 reported by Kropholler et al. for measurements obtained in arterial blood (*22*).

In Figure 2, measurements of the parent fraction in plasma from previous studies with ^{11}C-(*R*)-PK11195 in humans (*32–35*) are shown in comparison with our results. Our data can be equally described by a single exponential; however, the absolute values measured in arterialized venous plasma are only about 60% of the average parent fractions in arterial plasma previously published.

We have tested the most appropriate compartmental model (data not shown), and our data are in keeping with the findings of Kropholler et al. (*22*) in the knee joint. The reversible 1-tissue, 2-rate-constant compartmental model with a free blood volume term has proven satisfactory to describe the kinetics in the vessel wall; conversely, other models with more parameters do not provide fits that are significantly superior.

The use of the BSIFs, either total plasma or parent plasma, to estimate the kinetic parameters in the 2 cohorts led to negative K_1 estimates and fractional blood volumes larger than 1 for the 3 aortic ROIs or the ROI drawn in the lung parenchyma. The result was negative V_T estimates for these regions. A partial explanation could be the use of arterialized venous blood, which is a dispersed representation of the true arterial IF such that the peak is flattened but the area under the curve preserved (*27*). Arterial sampling, although considered the gold standard for deriving arterial IF, is laborious and sensitive to errors, and we therefore elected to avoid arterial cannulation to prevent the potential complications related to this invasive procedure.

On the other hand, when using IDIFs to fit the time–activity curves of the same tissue regions, we obtained plausible estimates for K_1, blood volume, and V_T. More important, the use of the IDIFs instead of the BSIFs led to a better fit of the data, as was substantiated by the reduction of the sum of squared errors of the fit, thus identifying IDIF as the more appropriate IF for tracer kinetic modeling.

The comparison of the regional V_T estimates in the 2 cohorts of patients showed a slightly higher discriminatory power for the total plasma IF. The close similarity of the V_T estimates indicates the negligible effect of labeled metabolites in these 2 small cohorts of patients. The same conclusion was reached by Kropholler et al. in their study on the inflammation of knee joints in patients with rheumatoid arthritis using ^{11}C-(*R*)-PK11195 (*22*). The advantage of this approach is the simplification of the acquisition protocol, obviating the sampling and measurement of radiolabeled compounds in plasma. In addition to the small variability of the POB ratio, this simplified method using IDIF can be used for the quantitative analysis of dynamic ^{11}C-(*R*)-PK11195 studies in vasculitides.

The simplified SUV showed a good correlation with V_T total-plasma IDIF even though in this small cohort the discriminating power was not significant. Nevertheless, in a larger cohort of patients the semiquantitative evaluation with the target-to-background ratio has proven potentially valuable in clinical practice (*5*).

TABLE 2
Parameter Estimates of Reversible 1-Tissue-Compartment Model for Asymptomatic Patients

Region	IF	K_1 ($mL_{plasma} \cdot min^{-1} \cdot mL_{extravascular\ tissue}^{-1}$)	k_2 (min^{-1})	Blood volume	V_T ($mL_{plasma} \cdot mL_{extravascular\ tissue}^{-1}$)	Residual sum of square errors
Bone marrow	Total-plasma BSIF	0.111 ± 0.049	0.043 ± 0.013	0.196 ± 0.129	2.479 ± 0.513	3.569 ± 3.982
	Parent-plasma BSIF	0.151 ± 0.072	0.024 ± 0.010	0.171 ± 0.123	6.036 ± 0.749	3.911 ± 3.937
	Total-plasma IDIF	0.088 ± 0.034	0.039 ± 0.008	0.036 ± 0.055	2.510 ± 0.545	3.000 ± 2.925
	Parent-plasma IDIF	0.108 ± 0.045	0.017 ± 0.006	0.027 ± 0.058	6.017 ± 0.929	4.002 ± 2.583
Lung parenchyma	Total-plasma BSIF	−5.153 ± 10.313*	2.541 ± 4.829	1.292 ± 1.574*	−0.496 ± 1.075*	6.734 ± 5.159
	Parent-plasma BSIF	−0.173 ± 0.356*	0.379 ± 0.595	0.675 ± 0.342	−0.074 ± 0.329*	7.322 ± 5.364
	Total-plasma IDIF	0.036 ± 0.008	0.205 ± 0.066	0.280 ± 0.112	0.187 ± 0.042	3.225 ± 3.375
	Parent-plasma IDIF	0.034 ± 0.005	0.120 ± 0.046	0.287 ± 0.114	0.313 ± 0.121	3.607 ± 3.747
Mean of aortic walls (descending, arch, ascending)	Total-plasma BSIF	−3.805 ± 5.076*	2.222 ± 2.130	1.839 ± 1.465*	−0.710 ± 1.123*	22.412 ± 22.544
	Parent-plasma BSIF	−0.445 ± 0.579*	0.577 ± 0.513	1.016 ± 0.522*	−0.133 ± 0.958*	30.433 ± 21.391
	Total-plasma IDIF	0.014 ± 0.008	0.050 ± 0.023	0.449 ± 0.121	0.275 ± 0.119	6.863 ± 5.327
	Parent-plasma IDIF	0.016 ± 0.009	0.030 ± 0.012	0.449 ± 0.120	0.580 ± 0.248	6.829 ± 5.269

*Blood volume (bv) > 1, K negative, V_T negative.
Data are mean ± SD (n = 4). For all regions considered, kinetic parameters were computed for 4 BSIFs and IDIFs.

FIGURE 4. V_T for aortic wall. Mean values with their SD for the 4 asymptomatic and 3 symptomatic patients are given. Continuous line = V_T parent-plasma IDIF. Hatched line = V_T total-plasma IDIF. *P = 0.009 vs. total plasma asymptomatic patients. †P = 0.018 vs. parent plasma asymptomatic patients.

Other less selective tracers, such as ^{18}F-FDG, have been used in the clinical setting to discriminate active inflammation and macrophage-rich infiltrates in large-vessel vasculitides (*1*); however, to improve the sensitivity in the case of smaller lesions, it might be more suitable to quantify glucose transport K_i with partial-volume correction as recently described by Izquierdo-Garcia et al. in inflamed carotid atherosclerotic plaques (*36*). In a retrospective study in patients with prostate cancer, Kato et al. have proposed ^{11}C-choline as a diagnostic tool potentially quantifiable in aortic atherosclerotic lesions (*37*).

In the thin aortic arterial wall, partial-volume effects can hamper the recovery of the true radioactivity; partial-volume correction is attained in this model through the use of the free blood volume term, which accounts for spillover from the blood pool into target regions. Partial-volume effect should affect both asymptomatic and symp-

FIGURE 5. (A) Scatterplot between V_T total-plasma IDIF and SUV. $y = 0.5793 + 1.068x$; R = 0.79. (B) Scatterplot between V_T parent plasma IDIF and SUV. $y = 0.7574 + 0.2846x$; R = 0.52.

tomatic patients to the same extent and is unlikely to account for the differences observed between the 2 cohorts.

Further studies on larger cohorts implementing reconstruction-based partial-volume correction and respiration-gated acquisitions are warranted to minimize the blurring effect of breathing on small lesions and to explore the suitability of ^{11}C-(*R*)-PK11195 to monitor the course of vasculitides and disclose clinical remission after therapeutic interventions.

ACKNOWLEDGMENTS

Oliver Gaemperli was financially supported by the Swiss National Science Foundation (SNSF). We are thankful to Hammersmith Imanet radiographers Andrew Blyth, Hope McDevitt, and Andreanna Williams and to Safiye Osman for their excellent technical support.

REFERENCES

1. Blockmans D, Bley T, Schmidt W. Imaging for large-vessel vasculitis. *Curr Opin Rheumatol.* 2009;21:19–28.
2. Webb M, Chambers A, Al-Nahhas A, et al. The role of ^{18}F-FDG PET in characterising disease activity in Takayasu arteritis. *Eur J Nucl Med Mol Imaging.* 2004;31:627–634.
3. Rudd JH, Warburton EA, Fryer TD, et al. Imaging atherosclerotic plaque inflammation with [^{18}F]-fluorodeoxyglucose positron emission tomography. *Circulation.* 2002;105:2708–2711.
4. Kobayashi Y, Ishii K, Oda K, et al. Aortic wall inflammation due to Takayasu arteritis imaged with ^{18}F-FDG PET coregistered with enhanced CT. *J Nucl Med.* 2005;46:917–922.
5. Pugliese F, Gaemperli O, Kinderlerer AR, et al. Imaging of vascular inflammation with [^{11}C]-PK11195 and PET/CT angiography. *J Am Coll Cardiol.* 2010; 56:653–661.
6. Papadopoulos V, Baraldi M, Guilarte TR, Knudsen TB, Lacapère JJ, Lindemann P. Translocator protein (18 kDa): new nomenclature for the peripheral-type benzodiazepine receptor based on its structure and molecular function. *Trends Pharmacol Sci.* 2006;27:402–409.
7. Zavala F, Haumont J, Lenfant M. Interaction of benzodiazepines with mouse macrophages. *Eur J Pharmacol.* 1984;106:561–566.
8. Zavala F, Lenfant M. Benzodiazepines and PK 11195 exert immunomodulating activities by binding on a specific receptor on macrophages. *Ann N Y Acad Sci.* 1987;496:240–249.
9. Banati RB, Newcombe J, Gunn RN, et al. The peripheral benzodiazepine binding site in the brain in multiple sclerosis: quantitative in vivo imaging of microglia as a measure of disease activity. *Brain.*2000;123:2321–2337.
10. Cagnin A, Brooks DJ, Kennedy AM, et al. In-vivo measurement of activated microglia in dementia. *Lancet.* 2001;358:461–467.
11. Gerhard A, Schwarz J, Myers R, Wise R, Banati RB. Evolution of microglial activation in patients after ischemic stroke: a [^{11}C](R)-PK11195 PET study. *Neuroimage.* 2005;24:591–595.
12. Junck L, Olson JMM, Ciliax BJ, et al. PET imaging of human gliomas with ligands for the peripheral benzodiazepine binding site. *Ann Neurol.* 1989;26:752–758.
13. Pappata S, Levasseur M, Gunn RN, et al. Thalamic microglial activation in ischemic stroke detected in vivo by PET and [^{11}C]PK1195. *Neurology.* 2000;55:1052–1054.
14. van Berckel BN, Bossong MG, Boellaard R, et al. Microglia activation in recent-onset schizophrenia: a quantitative (R)-[^{11}C]PK11195 positron emission tomography study. *Biol Psychiatry.* 2008;64:820–822.
15. Kropholler MA, Boellaard R, Schuitemaker A, Folkersma H, van Berckel BN, Lammertsma AA. Evaluation of reference tissue models for the analysis of [^{11}C](R)-PK11195 studies. *J Cereb Blood Flow Metab.* 2006;26:1431–1441.
16. Kropholler MA, Boellaard R, van Berckel BN, et al. Evaluation of reference regions for (R)-[^{11}C]PK11195 studies in Alzheimer's disease and mild cognitive impairment. *J Cereb Blood Flow Metab.* 2007;27:1965–1974.
17. Turkheimer FE, Edison P, Pavese N, et al. Reference and target region modeling of [^{11}C]-(R)-PK11195 brain studies. *J Nucl Med.* 2007;48:158–167.
18. Tomasi G, Edison P, Bertoldo A, et al. Novel reference region model reveals increased microglial and reduced vascular binding of ^{11}C-(R)-PK11195 in patients with Alzheimer's disease. *J Nucl Med.* 2008;49:1249–1256.
19. Kropholler MA, Boellaard R, Schuitemaker A, et al. Development of a tracer kinetic plasma input model for (R)-[11C]PK11195 brain studies. *J Cereb Blood Flow Metab.*2005;25:842–851.
20. Jones HA, Marino PS, Shakur BH, Morrell NW. In vivo assessment of lung inflammatory cell activity in patients with COPD and asthma. *Eur Respir J.* 2003;21:567–573.
21. Branley HM, du Bois RM, Wells AU, Jones HA. PET scanning of macrophages in patients with scleroderma fibrosing alveolitis. *Nucl Med Biol.* 2008;35:901–909.
22. Kropholler MA, Boellaard R, Elzinga EH, et al. Quantification of (R)-[^{11}C] PK11195 binding in rheumatoid arthritis. *Eur J Nucl Med Mol Imaging.* 2009;36:624–631.
23. van der Laken CJ, Elzinga EH, Kropholler MA, et al. Noninvasive imaging of macrophages in rheumatoid synovitis using ^{11}C-(R)-PK11195 and positron emission tomography. *Arthritis Rheum.* 2008;58:3350–3355.
24. Charbonneau P, Syrota A, Crouzel C, Valois JM, Prenant C, Crouzel M. Peripheral-type benzodiazepine receptors in the living heart characterized by positron emission tomography. *Circulation.* 1986;73:476–483.
25. Kinahan PE, Rogers JG. Analytic 3D image reconstruction using all detected events. *IEEE Trans Nucl Sci.* 1989;36:964–968.
26. Iatrou M, Manjeshwar RM, Ross SG. Implementation and analysis of a 3D iterative reconstruction algorithm for the Discovery ST PET/CT scanner [abstract]. *J Nucl Med.* 2005;46(suppl):56P.
27. van der Weerdt AP, Klein LJ, Visser CA, Visser FC, Lammertsma AA. Use of arterialised venous instead of arterial blood for measurement of myocardial glucose metabolism during euglycaemic-hyperinsulinaemic clamping. *Eur J Nucl Med Mol Imaging.* 2002;29:663–669.
28. Hinz R, Turkheimer FE. Determination of tracer arrival delay with spectral analysis. *IEEE Trans Nucl Sci.* 2006;53:212–219.
29. Budinger FT, Huesman RH, Knittel B, Friedland RP, Derenzo SE. Physiological modeling of dynamic measurements of metabolism using positron emission tomography. In: Greitz T, Ingvar DH, Widen L, eds. *The Metabolism of the Human Brain Studied with Positron Emission Tomography.* New York, NY: Raven Press; 1984:165–183.
30. Fujimura Y, Hwang PM, Trout H III, et al. Increased peripheral benzodiazepine receptors in arterial plaque of patients with atherosclerosis: an autoradiographic study with [^{3}H]PK11195. *Atherosclerosis.* 2008;201:108–111.
31. Gaemperli O, Boyle JJ, Rimoldi OE, Mason JC, Camici PG. Molecular imaging of vascular inflammation. *Eur J Nucl Med Mol Imaging.* 2010;37:1236.
32. De Vos F, Dumont F, Santens P, Slegers G, Dierckx R, De Reuck J. High-performance liquid chromatographic determination of [^{11}C]-1-(2-chlorophenyl)-N-methyl-N-(1-methylpropyl)-3-isoquinoline carboxamide in mouse plasma and tissue and in human plasma. *J Chromatogr B Biomed Sci Appl.* 1999; 736:61–66.
33. Pike VW, Halldin C, Crouzel C, et al. Radioligands for PET studies of central benzodiazepine receptors and PK (peripheral benzodiazepine) binding sites: current status. *Nucl Med Biol.* 1993;20:503–525.
34. Roivainen A, Nagren K, Hirvonen J, et al. Whole-body distribution and metabolism of [N-methyl-^{11}C](R)-1-(2-chlorophenyl)-N-(1-methylpropyl)-3-isoquinolinecarboxamide in humans: an imaging agent for in vivo assessment of peripheral benzodiazepine receptor activity with positron emission tomography. *Eur J Nucl Med Mol Imaging.* 2009;36:671–682.
35. Greuter HNJM, van Ophemert PLB, Luurtsema G, et al. Optimizing an online SPE-HPLC method for analysis of (R)-[^{11}C]1-(2-chlorophenyl)-N-methyl-N-(1-methylpropyl)-3-isoquinolinecarboxamide [(R)-[^{11}C]PK11195] and its metabolites in humans. *Nucl Med Biol.* 2005;32:307–312.
36. Izquierdo-Garcia D, Davies JR, Graves MJ, et al. Comparison of methods for magnetic resonance-guided [18-F]fluorodeoxyglucose positron emission tomography in human carotid arteries: reproducibility, partial volume correction, and correlation between methods. *Stroke.* 2009;40:86–93.
37. Kato K, Schober O, Ikeda M, et al. Evaluation and comparison of ^{11}C-choline uptake and calcification in aortic and common carotid arterial walls with combined PET/CT. *Eur J Nucl Med Mol Imaging.* 2009;36:1622–1628.